Journal of
Synchrotron
Radiation

ISSN 0909-0495

Received 28 May 2004
Accepted 5 January 2005

Parameters affecting the X-ray dose absorbed by macromolecular crystals

James W. Murray,[a]‡ Enrique Rudiño-Piñera,[a,b] Robin Leslie Owen,[a] Martin Grininger,[c] Raimond B. G. Ravelli[d] and Elspeth F. Garman[a]*

[a]Laboratory of Molecular Biophysics, Department of Biochemistry, Oxford University, Rex Richards Building, South Parks Road, Oxford OX1 3QU, UK, [b]Departamento de Medicina Molecular y Bioprocesos, Instituto de Biotecnología, Universidad Nacional Autónoma de México, PO Box 510-3, Cuernavaca, MOR 62271, México, [c]Max-Planck-Institut für Biochemie, Am Klopferspitz 18, 82152 Martinsried bei München, Germany, and [d]European Molecular Biology Laboratory (EMBL) Grenoble Outstation, 6 rue Jules Horowitz, BP 181, F38042 Grenoble Cedex 9, France.
E-mail: elspeth@biop.ox.ac.uk

The lifetime of a macromolecular crystal in an X-ray beam is assumed to be limited by the absorbed dose. This dose, expressed in Gray (Gy = J kg^{-1}), is a function of a number of parameters: the absorption coefficients of the constituent atoms of the crystal, the number of molecules per asymmetric unit, the beam energy, flux, size and profile, the crystal size, and the total irradiation time. The effects of these variables on the predicted absorbed dose, calculated using the program *RADDOSE*, are discussed and are illustrated with reference to the irradiation of a selenomethionine protein crystal of unknown structure. The results of *RADDOSE* can and will in the future be used to inform the data collection procedure as it sets a theoretical upper limit on the total exposure time at a certain X-ray source. However, as illustrated with an example for which the experimental data are compared with prediction, the actual lifetime of a crystal could become shorter in those cases where specific damage breaks down crucial crystal contacts.

Keywords: absorbed dose; Henderson limit; X-ray diffraction; radiation damage; dodecin.

1. Abbreviations

EM: electron microscopy.
MAD: multiple anomalous dispersion.
MIR: multiple isomorphous replacement.
PIXE: particle-induced X-ray emission.
SAD: single anomalous dispersion.

2. Introduction

In order to characterize the radiation damage process induced by an X-ray beam in a cryocooled macromolecular crystal, it is necessary to know the absorbed dose: the energy deposited per unit mass of the crystal (units Gy = J kg^{-1}). The damage suffered by the crystal is a function of this absorbed dose, since the energy dissipated in a cryocooled crystal will cause a variety of processes, including covalent bond breakage, ionization and heat production. These processes will result in degradation of the crystalline order and thus a reduction in its diffracting power. After a finite absorbed dose, the crystal diffraction will have deteriorated to the point where, depending on the purpose of the data collection (*e.g.* experimental phasing, high-resolution data collection or molecular replacement), further data collection will be fruitless.

The dose can be calculated from knowledge of both the absorption coefficients of the atoms present in the crystal and the experimental conditions (beam size, profile, energy and flux; crystal size and the irradiation time). The incident X-ray beam energy has a pivotal influence on the absorption coefficient of an atom; above an absorption edge the absorption coefficient can be several times larger than below, depending on the kind of edge. This phenomenon allows experimenters to choose the incident energy according to their purpose in data collection: below the edge for high-resolution data collection or at the peak if maximum anomalous signal (at the price of maximal absorption) is desired (Arndt, 1984).

A computer program, *RADDOSE*, for performing absorbed dose calculations has been reported (Murray *et al.*, 2004); here we use this program to highlight the factors important for the absorbed dose. For the calculations reported in this paper, *RADDOSE* was modified to include the effect of energy escaping from the crystal in the form of fluorescent X-rays produced by the interaction of photoelectrons with

‡ Current address: Institute of Cell and Molecular Biosciences, Faculty of Medical Sciences, University of Newcastle, Framlington Place, Newcastle-upon-Tyne NE2 4HH, UK.

heavier elements, for which the fluorescent X-ray production cross section is significant.

We illustrate the effects of incident X-ray energy, crystal content, the number of molecules in the asymmetric unit and crystal size on the predicted lifetimes for an as yet unsolved selenomethionine (SeMet)-containing protein crystal, and we compare the prediction of *RADDOSE* with the experimentally observed lifetime of a crystal of dodecin, a protein of known structure. Data from these latter crystals have been collected on the high-brilliance undulator beamline ID14-4 at the ESRF.

3. Interactions of X-rays with matter

X-rays interact with matter in three ways. The X-ray photons may be absorbed *via* the photoelectric effect, scattered inelastically (Compton scattering) or scattered elastically (Thomson scattering). Only the last of these contributes to the useful part of the observed diffraction pattern. The dominant interaction at energies typically used in macromolecular crystallography is the photoelectric effect, which accounts for more than 80% of the total interaction, with around 8% being due to Compton scattering. Therefore most of the X-rays interacting with the crystal deposit their energy into it, causing 'radiation damage'. Radiation damage puts a fundamental limit on the diffraction experiment.

The radiation dose deposited in a crystal is defined as the energy absorbed per unit mass. The most commonly quoted theoretical limit to the dose that may be deposited in a cryo-cooled protein crystal held at or around 100 K is that of Henderson (1990). Using the observation that, for a very wide variety of organic and biological samples held at 77 K, 5 e Å^{-2} of energy 100 keV cause an electron diffraction pattern to fade to half its original intensity, he computed the amount of energy deposited per unit mass by the electrons, assuming an average penetration depth of 100 µm (typical of a protein crystal embedded in glucose) to 140 µm (vitreous ice). He obtained a dose of 5×10^7 Gy, but argued that in the first part of the dose-depth curve this value might be two to three times less, say 2×10^7 Gy. For EM, some individual electron microscopes are calibrated to allow an accurate calculation of the dose delivered to the sample under investigation. Hitherto, however, no analogue exists in the field of macromolecular crystallography.

For kinematic scattering (*i.e.* no dynamical scattering) in a typical protein crystal of 100 µm in thickness at an X-ray energy of 12.7 keV, around 98% of the incident photons pass through the crystal without interacting. Of the 2% that do interact, about 84% are absorbed *via* the photoelectric interaction, and the remaining 16% are split about equally between the coherent and incoherent interactions. Thus, in total, less than 0.2% of the incident photons are diffracted by the crystal.

4. *RADDOSE*

We have written a computer program, *RADDOSE* (available from the authors on request), to estimate the absorbed dose and hence to calculate (among other quantities) the expected crystal lifetime given the beam parameters and the contents of the crystal unit cell. The program is optimized for macromolecular crystals, and implements a simple model of absorption and temperature increase (Kuzay *et al.*, 2001) (see Fig. 1). The results from *RADDOSE* are somewhat limited, as they give an estimate of the total lifetimes of crystals based on the Henderson limit and therefore provide a maximum value of the dose that the crystal will tolerate. However, the times obtained can be a useful aid while planning a data collection strategy.

To estimate the absorbed dose from the incident flux, the crystal size and composition must be known. The approximate crystal dimensions may be derived from an appropriate graticule on the beamline camera used to centre the crystal (Andrey *et al.*, 2004). The atomic composition may be estimated from the amino-acid and nucleotide composition of the crystal and the known components of the solvent (cryoprotectant buffer or mother liquor). If desired, the absorption coefficients of anomalously scattering atoms may be corrected using a normalized experimental fluorescence scan, as produced by the program *CHOOCH* (Evans & Pettifer, 2001) for input into *RADDOSE*.

All this information may be used to estimate the time taken to reach a given absorbed radiation dose and other parameters associated with absorption. These include the dose per data set, the dose per image, the maximum predicted temperature rise (using a specific heat capacity, c_p, of 5×10^2 J K^{-1} kg^{-1} and a heat transfer coefficient, h, of 320 W m^{-2} K^{-1}) and the number of photons absorbed per unit cell at the specified dose limit (2×10^7 Gy is the default dose limit).

A useful quantity, also calculated by *RADDOSE*, which relates the diffraction to the absorbed dose, is the diffracted intensity per dose unit, the so called 'diffraction-dose efficiency', $I_{\rm DE}$ (Murray *et al.*, 2004). $I_{\rm DE}$ will obviously be higher for crystals that do not contain anomalous scatterers either in the protein or in the solvent, so more information per absorbed photon will be obtained in this case than for a crystal that includes heavier element components.

Several assumptions are made in *RADDOSE* when calculating the absorbed dose. Firstly, it is presumed that the rate of energy deposition does not affect the radiation dose limit, which is experimentally thought to be the case below a flux of 10^{15} photons s^{-1} mm^{-2} (Sliz *et al.*, 2003). Secondly, no account is taken of the rotation of the crystal in the beam during the data collection, so if the crystal is larger than the beam, new parts of the crystal will be irradiated as it rotates. The dose calculation is therefore valid only for the part of the crystal that stays in the beam throughout the data collection. Finally, *RADDOSE* uses the photoelectric cross sections to calculate the absorption coefficient, and thus photons that are Compton scattered are neglected since they contribute little to the absorption. This simplification leads to a small underestimate of the absorbed dose. These processes do, however, contribute to the overall attenuation of the beam and are included in the total cross section used to calculate the attenuation coefficient.

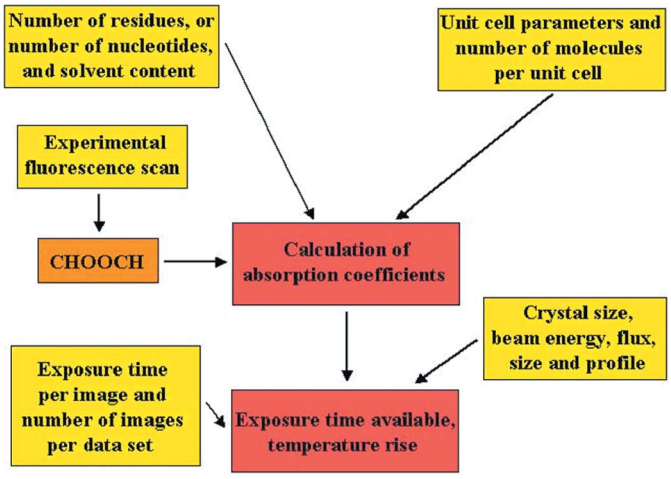

Figure 1
A schematic diagram to show the flow of data through *RADDOSE*. Yellow boxes represent input by the user, red boxes indicate results output by *RADDOSE* and the orange box represents the use of another program. The *RADDOSE* output also includes the dose per image, the number of photons absorbed per unit cell, the diffracted intensity per absorbed dose, the attenuation and absorption coefficients, and the percentage of the incident beam absorbed by the crystal.

In contrast to the results from *RADDOSE* reported by Murray *et al.* (2004), the escape from the crystal of fluorescent X-rays produced in conjunction with the photoelectrons has been taken into account for the calculations presented here. For elements heavier than sulfur, the fluorescent yield becomes significant above the absorption edge for that element. As a result, less energy is deposited in the crystal and thus the predicted lifetime is longer than if the escape of fluorescent X-rays is not taken into account.

In the future, dose calculations will be included as an integral part of an automated structure solution pipeline, which has a strategy decision tree to determine the course of the diffraction experiment. In particular, *RADDOSE* is being incorporated into the DNA automation project (Leslie *et al.*, 2002; Arzt *et al.*, 2004).

5. Flux calibration

It is absolutely necessary to know the beam flux in order to calculate the dose absorbed by a sample exposed to X-rays. Calibration of the flux can be problematic, as the flux varies for a particular beamline with X-ray energy, beam profile, slit settings, attenuators, undulator gap and the storage ring current. In order to compare predicted lifetimes calculated by *RADDOSE* with experimental results, we have used a calibrated X-ray sensitive photodiode (Hamamatsu, model No. S3204-08) to measure the flux regularly at beamline ID14-4 at the ESRF (P. Theveneau, personal communication). The current recorded from the photodiode may then be calibrated against the pin-diode or ion-chamber readings on the beamline. Diodes need to be calibrated against a wide range of energies (MAD beamlines) and the calibration must be checked regularly as it is subject to the particular beamline settings and drift. It can be difficult to find out what the flux was after the experiment, and until flux measurements become routine this situation is likely to persist.

6. Crystal content

For absorbed dose calculations, the contents and size of the crystal unit cell must be known, including the approximate concentrations of the solvent atoms, which are most conveniently quoted as millimolar values. The software can then fill the volume not occupied by protein with water and solvent at the right concentration, and the overall absorption coefficients can be calculated. Since the atomic absorption coefficients increase in approximate proportion to the fourth power of the atomic number, the presence of heavier elements has a disproportionate effect on the absorbed dose. The dose will be increased by a heavy atom soaked in to the crystal to perform an SIR/MIR (*e.g.* Hg, Pt, Au or Pb) or SAD/MAD experiment, and thus the crystal lifetime will be diminished. Similarly, any endogenous heavy atoms will increase the absorbed dose (*e.g.* Cu, Fe or Se in SeMet). The imaginary component of the anomalous scattering factor, f'', is directly proportional to the photoelectric cross section of an atom. Therefore, the more favourable an atom is for anomalous phasing, the greater is the contribution of this atom to the absorbed dose.

This phenomenon is illustrated in Fig. 7 of Murray *et al.* (2004), which compares the diffraction-dose efficiency for a native, a selenomethionine derivative, an NaI-soaked and a NaBr-soaked xylanase crystal. The decrease in diffraction-dose efficiency for the halide-soaked crystals implies that backsoaking would be beneficial, as it would minimize the number of non-specifically bound heavy scatterers (Garman & Murray, 2003). For instance, results from *RADDOSE* show that, for a 5 m*M* gold-soaked $CD55_{34}$ (Williams *et al.*, 2003) crystal with three gold sites per monomer and one monomer (125 amino acids) per asymmetric unit, backsoaking could increase the lifetime of the crystal (at 13.2 keV beam energy) by around 10%, and for a platinum derivative (two sites per monomer) by approximately 15%.

The relative contributions of component atoms to the absorption and the large effect of the presence of heavier elements in a crystal are illustrated in Fig. 2. The relative absorptions at different incident energies are shown for both a native and an SeMet-containing crystal of a protein of unknown structure which is currently under investigation.

The protein used for these calculations has 398 residues (mass 45 kDa), of which three are cysteines and 12 are methionines (excluding the N-terminal methionine residue). In *RADDOSE*, each amino acid is assumed to have five C atoms, 1.35 N atoms, 1.5 O atoms and eight H atoms. For the SeMet crystals, the mass ratio of sulfur to selenium in the crystal was measured using microPIXE (Garman, 1999), and the results indicated that there were 5.0 ± 0.4 S atoms to every 10.0 ± 0.4 Se atoms per protein molecule, *i.e.* 83% of the sulfur in the methionines was replaced by selenium. Thus, in the *RADDOSE* calculations, five S and ten Se atoms were included per monomer. Crystals were obtained under several conditions containing acetate buffer, sodium phosphate and

Table 1
The different possible numbers of monomers in the unit cell for example 1 (SeMet *P*1 protein crystal, see text) directly affects the time taken to reach the Henderson limit.

Calculations were performed at the peak Se X-ray energy V_m and the solvent content was calculated using *MATTHEWS_COEF* from the CCP4 suite (Matthews, 1968).

Number of monomers in the unit cell	V_m (Å^3 Da^{-1})	Solvent content (%)	Relative time(s) to reach a dose of 2×10^7 Gy
1	12.07	89.8	1.11
2	6.03	79.6	1.07
3	4.02	69.4	1.03
4	3.02	59.2	1.0
5	2.41	49.0	0.97
6	2.01	38.9	0.95
7	1.72	28.7	0.92
8	1.51	18.5	0.90

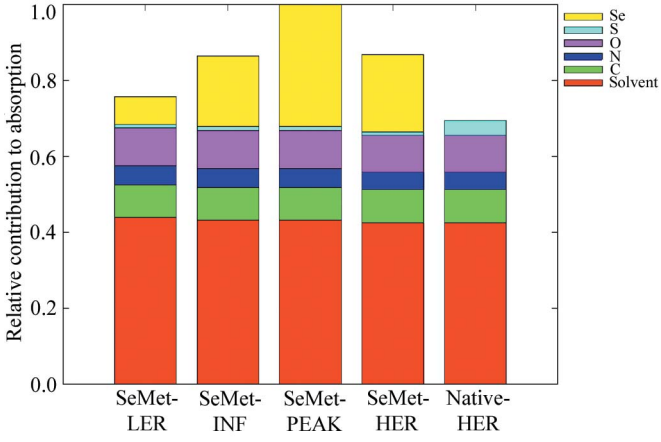

Figure 2
A histogram to show the contribution to absorption by atom type at different energies for SeMet and native protein crystals. The contribution from H atoms is negligible. (LER: lower-energy remote; INF: inflection point energy; HER: high-energy remote).

PEG MME 5000 (pH range between 6 and 7) as sitting- or hanging-drop experiments at 298 K. Those grown in 200 m*M* sodium acetate, pH 6.2, 100 m*M* sodium phosphate and 10% PEG MME 5000 are being used for structural studies, so these solvent conditions (300 m*M* Na^+ and 100 m*M* PO_4^-) were used for the calculations presented in Fig. 2.

The space group of these crystals appears to be *P*1, with unit-cell parameters of $a = 60.1$ Å, $b = 84.0$ Å, $c = 109.7$ Å, $\alpha = 107.2^\circ$, $\beta = 97.2^\circ$ and $\gamma = 93.4^\circ$. With these cell dimensions, there could theoretically be between one and eight molecules in the unit cell, giving a V_m of between 1.5 and 12.1 Å^3 Da^{-1} and a solvent content of between 18.5 and 89.8%, respectively (see Table 1). With four protein molecules in the unit cell, the solvent content is 59.2% ($V_m = 3.0$ Å^3 Da^{-1}), which is within the range of the majority of protein crystals, and so this value was used unless otherwise stated.

It can be seen from Fig. 2 that, regardless of the X-ray energy, the absorption of the native crystal is always lower than that of an SeMet-containing crystal, solely as a result of the presence of the Se atoms.

Table 2
The variation in relative diffracted dose efficiency below, on and above the selenium edge, as calculated by *RADDOSE* for a *P*1 SeMet crystal.

The dose efficiency (I_{DE}) is taken relative to that of the peak (see text).

Protein	Data set	Energy (keV)	Relative dose efficiency
SeMet	Low-energy remote	12.6000	1.34
SeMet	Inflection	12.6609	1.25
SeMet	Peak	12.6634	1.0
Native	Peak	12.6634	1.42
SeMet	High-energy remote	12.7200	1.13
Native	High-energy remote	12.7200	1.42

7. Number of molecules in the asymmetric unit

The number of molecules per asymmetric unit is sometimes not definitely known until structure solution is fairly well advanced. Thus all other possible values of the number of monomers in the unit cell have been used to illustrate the consequence of possible errors in this assignment. In going from one to eight monomers per unit cell, the time available before the Henderson limit is reached decreases by approximately 20%, as can be seen from Table 1. Thus lack of knowledge of the exact contents of the unit cell will give a corresponding uncertainty in the calculated absorbed dose.

8. Beam energy

If an anomalous scatterer is present, the absorbed dose will be much lower at an energy below the absorption edge of that atom than above it, and thus the relative dose efficiency for the crystal will be lower above the edge. This fact is illustrated in Table 2 for the same SeMet crystal; it is evident that, for the same dose, 34 and 13% more data can be obtained at the low- and high-energy remote energies, respectively, compared with the peak. A large contribution is made to the total absorption cross section by the ten Se atoms per protein monomer, particularly around and above the peak energy (see Fig. 2).

An empirical correction to the absorption of the Se atoms was made using the experimental fluorescence scan (see Fig. 3) collected from the protein crystal prior to collection of the first image. Note that the escape of fluorescent selenium X-rays possible above the absorption edge has been taken into account. The energy they carry away results in a 26% decrease in the calculated dose above the absorption edge.

If, after calculating the predicted lifetime with *RADDOSE* at a certain attenuation, it is clear that a three or even two energy MAD experiment could not be collected from a single crystal with this attenuation, the data collection strategy should be re-evaluated. It may be that even obtaining just a peak wavelength SAD data set is problematic without reducing the exposure time or further attenuating the beam flux for the same exposure time. Judging the trade-off between the number of diffracted photons and the absorbed dose is likely to be particularly difficult for weakly diffracting crystals, where the resolution of the data must be sufficient for structure solution. If the crystal is larger than the beam, it can be

Table 3
The effect of crystal depth on the absorbed dose for the *P*1 SeMet protein crystal (see text).

Calculations were performed at the peak Se X-ray energy. The relative time taken for the predicted absorbed dose to reach 2×10^7 Gy is given, normalized for the case of a 100 μm-deep crystal.

Crystal depth (μm)	Normalized relative absorbed energy	Normalized relative dose	Relative time(s) to reach a dose of 2×10^7 Gy
20	1.0	1.00	0.99
50	2.5	1.00	0.99
100	5.0	0.99	1.0
200	9.8	0.97	1.01
500	23.8	0.93	1.06
1000	43.3	0.87	1.14

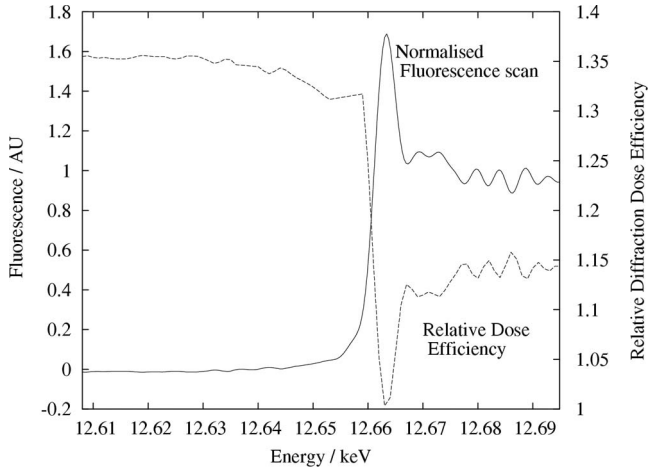

Figure 3
A graph to show the experimental fluorescence scan of a protein crystal with ten Se atoms per 45 kDa monomer (see text), and the calculated diffraction dose efficiency (normalized to 1 at the peak energy of 12.663 keV).

translated in order to collect later wedges of data from fresh parts of the crystal.

In Table 2, the results from *RADDOSE* have been quoted in terms of the relative dose efficiency, which is the number of diffracted photons per absorbed dose, $I_{\rm DE}$ (Murray *et al.*, 2004), normalized to the value at the peak energy. It can be seen that for the SeMet crystal the dose efficiency is highest for the low-energy remote energy, and is in fact 33% higher than that at the peak energy. If the phasing signal is sufficient, it might be possible to collect SAD data above the peak, where absorption is smaller, and thus higher redundancy can be obtained for the same total dose. If experimental phases were not required, an energy below the absorption edge might be the most desirable, as 33% more diffraction data can be collected before reaching the same absorbed dose. The native crystal has a longer predicted lifetime in the beam at all energies, and thus if the crystals are of comparable diffraction quality to the SeMet crystals the native should be used to collect the highest-resolution data set (see Table 2).

Radiation damage causes structural changes and cell expansion during data collection and thus induces non-isomorphism as the experiment proceeds. The resulting diffracted intensity changes add systematic errors to the data and also increase the statistical errors as the average of the reflection intensities decreases. These errors can become larger than the anomalous signal. In fact these effects are thought to be the cause of a significant number of failed MAD structure determinations. We note that the cell expansion appears to be crystal dependent (Murray & Garman, 2002; Ravelli *et al.*, 2002).

The results above illustrate how dose calculations prior to data collection might inform the best strategy for obtaining the maximum amount of data from a given crystal.

9. Crystal size

If the dimensions of the crystal perpendicular to the beam are X and Y then if the beam area, A, is smaller than XY, the absorbed dose will be independent of X and Y. If the beam is larger than XY, proportionally fewer photons will pass through the crystal, reducing the amount of absorbed energy by a factor XY/A, assuming a uniform beam intensity.

For a constant crystal depth, Z, the crystal volume will be proportional to XY. Thus the absorbed dose, expressed as the number of absorbed photons times their energy, divided by the crystal volume times its density (*i.e.* the crystal mass), stays constant.

The dose absorbed by a crystal is almost independent of the crystal depth, Z, through which the beam passes. This is because the absorption path length of the crystal for 8–14 keV X-rays is large compared with typical crystal sizes. Some examples of the relative absorption for different crystal depths of the SeMet-containing crystal already described are shown in Table 3. The attenuation coefficient is taken to be 0.39 $\rm mm^{-1}$ and the crystal is entirely illuminated by a beam of energy 12.663 keV (the selenium edge). The content of the crystal was assumed to be four monomers. For crystal depths of 20–1000 μm the dose decreases by only 14% compared with a 50-fold variation in volume and a 43-fold variation in energy absorbed. This result is slightly counterintuitive but is attributable to the fact that dose is equivalent to the specific absorbed energy, and that the beam is attenuated as it passes through the crystal, resulting in a lower average dose. Note that the above discussion and calculations do not take the rotation of the crystal during the data collection into account. If the crystal is larger than the beam in X and Y, part of the volume seen by the beam will be fresh until 180° has been swept out, and this factor will reduce the absorbed dose.

The question arises as to whether there is a minimum useful crystal size. This issue has been addressed by Gonzalez & Nave (1994), Neutze *et al.* (2000), Teng & Moffat (2000), Glaeser *et al.* (2000) and Sliz *et al.* (2003), who all estimated different minimum crystal sizes dependent on the protein in question and the criteria set for useful data. The issue of minimum crystal size is very important in view of current developments towards high-throughput crystallography at an increasing number of facilities. Resolving these issues requires better definition of 'useful data' *versus* dose absorbed. We

hope that the integration of *RADDOSE* into these pipelines will assist in this aim.

10. Comparison of dose calculation with observed lifetime: specific damage and dodecin

The dose limit of Henderson is based solely on the amount of energy deposited in the crystal per unit mass and does not take specific structural damage into account. Specific damage in this context is defined as structural alterations upon X-ray damage that are observable in the electron-density difference map between an initial data set and a subsequent one. Well known specific damage sites are disulphide bonds and acidic side chains (Burmeister, 2000; Ravelli & McSweeney, 2000; Weik *et al.*, 2000). Breakage of these bonds could shorten the apparent lifetime of a crystal, especially when the most susceptible bonds are crucial for intra- or intermolecular packing.

An example of this problem was observed in crystals of dodecin. Dodecin is a 68 residue protein that assembles into dodecamers with 23-cubic point symmetry. Cubic crystals ($F4_132$) of dodecin (Bieger *et al.*, 2003) appear to be particular sensitive to radiation damage. Four successive data sets were collected from a dodecin crystal at the high-flux undulator MAD beamline ID14-4 at the ESRF. Table 4 gives the dose absorbed per data set, the resolution, $I/\sigma(I)$, the Wilson B factor as obtained using the CCP4 program *TRUNCATE* (French & Wilson, 1978) and the unit-cell axes. The dose was calculated using the program *RADDOSE* after calibration of the beamline diodes using a Hamamatsu windowless pin diode model No. S3204-08. The exposure time was 2 s per frame and a total of 40 frames of 1° each were collected per data set; the energy of the X-rays was 13.2 keV.

More than five data sets could have been collected before the Henderson limit was reached. Given the errors in flux calibration and dose calculation, this result seems to be in reasonable agreement with the results from the four data sets collected. However, the large unit-cell volume increase of about 1% per data set [as determined using *XDS* (Kabsch, 1988)], as well as the rapid decrease in the resolution of the diffraction when using only a moderate total exposure time per data set, raises the question of whether there is an additional factor that hastens the apparent rate of radiation damage for these crystals.

Refinement using *REFMAC* (Murshudov *et al.*, 1997) of the structure against the first data set and inspection of $F_o - F_o$ maps between the first and successive data sets show characteristic signs of specific damage on Gln68, Glu57, Asp25, Glu28 and Glu14. Of these residues, Glu57 plays a crucial role in the packing of the 12 monomers into a 89.3 kDa complex.

Fig. 4 shows the assembly of this complex. The dodecamer consists of four trimeric units. The intermolecular contacts within each trimer are very tight, as the three-stranded β sheet of each monomer extends to a five-stranded antiparallel β sheet (Bieger *et al.*, 2003). However, between the trimers, the contacts are less extensive. They consist of antiparallel main-chain–main-chain pairing (between Phe3-Lys5 of $\beta1$ and Leu7-Thr9 of $\beta1'$), as well as two salt bridges, between Glu57 and Lys5′, and Lys5 and Glu57′, where the prime (′) refers to a symmetry-related protein molecule.

Table 4
Several indicators of data quality for subsequent data sets collected from the same crystal of dodecin.

	Data set *A*	Data set *B*	Data set *C*	Data set *D*
Unit-cell axis *a* (Å)	142.61	143.70	144.20	144.49
Relative unit-cell volume	1.000	1.023	1.034	1.040
Resolution (highest shell) (Å)	1.7 (1.8–1.7)	1.9 (2.02–1.9)	2.1 (2.23–2.1)	2.3 (2.44–2.3)
Wilson *B* value† (Å^2)	22.5	26.8	32.5	36.1
$I/\sigma(I)$ (highest shell)	19.4 (5.2)	19.3 (5.9)	17.9 (5.9)	16.4 (5.4)
R value (highest shell) (%)	7.0 (40.9)	7.3 (37.4)	7.9 (36.2)	8.7 (38.5)

† Wilson scaling was carried out using reflections within the resolution range 3.3–2.3 Å.

Additionally, in the holoprotein state, incorporated flavin contributes to the stability of the dodecamer by mediating stacking interactions between W36 and W36′, and W36′ and W36, where again the prime refers to a symmetry-related protein molecule.

The decarboxylation of Glu57 appears as a 10σ peak in the $F_o - F_o$ map between data sets *A* and *C* and is the second highest peak in the difference Fourier map (Fig. 5). Upon decarboxylation, the salt bridges holding the trimers together are lost, and this process will highly destabilize the dodecameric structure. We believe that this factor could have direct consequences for the crystalline diffraction properties of these crystals, resulting in a much faster decay than predicted by the Henderson limit.

It remains an open question as to whether the enhanced sensitivity of dodecin crystals to radiation damage is exceptional or not. The small size of the protein, as well as the high symmetry within the dodecameric assembly, could make it particularly prone to the decarboxylation effects of one or two residues. However, even in large complexes, individual residues are sometimes found to make crucial crystallographic symmetry or non-crystallographic symmetry contacts, and it is possible that specific damage to these residues will also significantly shorten the apparent lifetime of those crystals.

The Henderson limit and the calculations as performed with *RADDOSE* will therefore only set an upper limit on the crystal lifetime. Extensive evaluation of the predicted *versus* the real lifetime of different crystals should indicate how often specific radiation damage in vital locations is likely to cause major discrepancies in real *versus* predicted lifetimes.

11. Conclusions

X-rays interact with matter in well defined and well characterized ways. Therefore, given the atomic composition of a macromolecular crystal, it is possible to model the absorption of radiation by the cryocooled crystal. We have implemented a

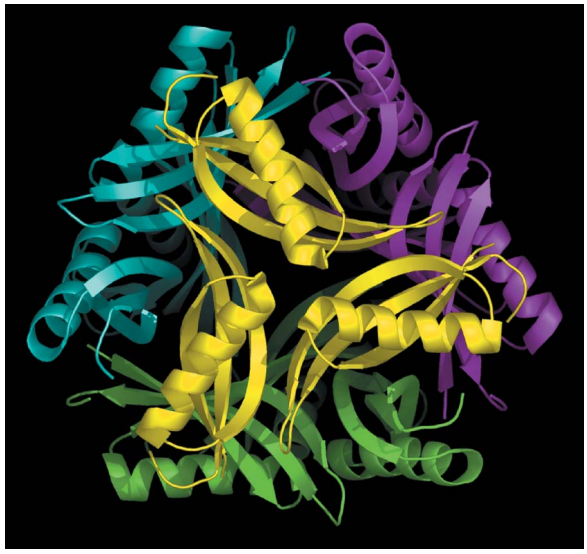

Figure 4
Quaternary packing of dodecin (PDB code: 1mog). The dodecameric packing of the 68-residue-long protein dodecin consists of four trimers, coloured orange, blue, cyan and marine.

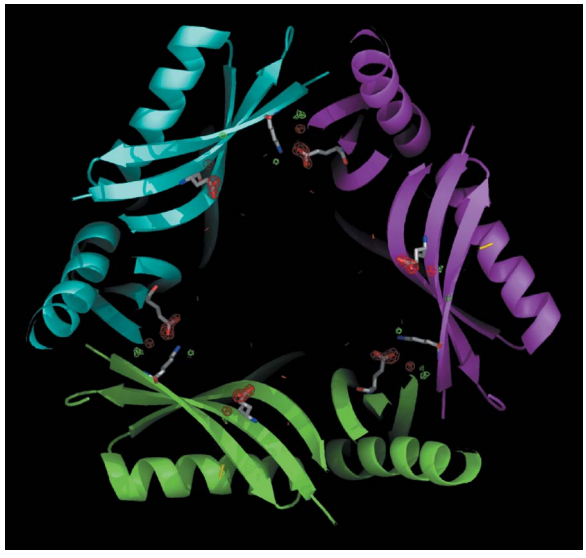

Figure 5
A salt bridge between Glu57 and Lys5′ stabilizes the packing of the trimers into the dodecamer. The carboxyl group of Glu57 is one of the most X-ray sensitive parts of the structure, as shown by an F_o (data set A) − F_o (data set C) difference map, contoured at $\pm 7\sigma$.

simple model of absorption, and hence radiation damage, as well as of the predicted temperature rise, in a computer program, *RADDOSE*. The program has been used to illustrate the effect of crystal composition, the number of molecules per asymmetric unit, the beam energy and the crystal size on the relative lifetime of an SeMet crystal of unknown structure. It should be noted here that the results of dose calculations also have a high dependency on the accuracy with which the settings on a particular beamline are known. Reliable values for parameters such as the beam area, profile and flux are crucial to allow a good estimation of the life expectancy of a protein crystal before the quality of the data is compromised by radiation damage.

In addition, it was shown how specific damage to crucial crystal contacts might accelerate the crystal decay beyond what is predicted by the program. We hope that the *RADDOSE* program will become a useful tool to macromolecular crystallographers both in optimizing data collection strategies and for future automated structure solution pipelines.

We gratefully acknowledge the staff of the EMBL Grenoble Outstation and the ESRF for support, maintenance and development of the JSBG beamlines, and the ESRF for beamtime under long-term project LS2047 and BAG projects MX-161 (Radiation Damage) and MX-197 (LMB Oxford). JWM was supported by an MRC studentship and visited the EMBL Grenoble Outstation under the EU Improving Human Potential Access to Research Infrastructures Programme HPRI-CT-1999-00022. RLO is supported by a BBSRC CASE studentship and ERP by the Programa de Apoyos para la Superación del Personal Académico (PASPA-UNAM) from the Universidad Nacional Autónoma de México.

References

Andrey, P., Lavault, B., Cipriani, F. & Maurin, Y. (2004). *J. Appl. Cryst.* **37**, 265–269.
Arndt, U. W. (1984). *J. Appl. Cryst.* **17**, 118–119.
Arzt, S., Beteva, A., Cipriani, F., Delageniere, S., Felisaz, F., Forstner, G., Gordon, E., Launer, L., Lavault, B., Leonard, G., Mairs, T., McCarthy, A., McCarthy, J., McSweeney, S., Meyer, J., Mitchel, E., Monaco, S., Nurizzo, D., Ravelli, R., Rey, V., Shepard, W., Spruce, D., Svensson, O. & Theveneau, P. (2004). *Prog. Biophys. Mol. Biol.* In the press.
Bieger, B., Essen, L. O. & Oesterhelt, D. (2003). *Structure*, **4**, 375–385.
Burmeister, W. P. (2000). *Acta Cryst.* D**56**, 328–341.
Evans, G. & Pettifer, R. F. (2001). *J. Appl. Cryst.* **34**, 82–86.
French, G. S. & Wilson, K. S. (1978). *Acta Cryst.* A**34**, 517.
Garman, E. (1999). *Structure*, **7**, R291–R299.
Garman, E. & Murray, J. W. (2003). *Acta Cryst.* D**59**, 1903–1913.
Glaeser, R., Facciotti, M., Walian, P., Rouhani, S., Holton, J., MacDowell, A., Celestre, R., Cambie, D. & Padmore, H. (2000). *Biophys. J.* **78**, 3178–3185.
Gonzalez, A. & Nave, C. (1994). *Acta Cryst.* D**50**, 874–877.
Henderson, R. (1990). *Proc. R. Soc. London Ser. B*, **241**, 6–8.
Kabsch, W. (1988). *J. Appl. Cryst.* **21**, 916–242.
Kuzay, T. M., Kazmierczak, M. & Hsieh, B. J. (2001). *Acta Cryst.* D**57**, 69–81.
Leslie, A. G. W., Powell, H. R., Winter, G., Svensson, O., Spruce, D., McSweeney, S., Love, D., Kinder, S., Duke, E. & Nave, C. (2002). *Acta Cryst.* D**58**, 1924–1928.
Matthews, B. W. (1968). *J. Mol. Biol.* **33**, 491–497.
Murray, J. & Garman, E. (2002). *J. Synchrotron Rad.* **9**, 347–354.
Murray, J. W., Garman, E. & Ravelli, R. (2004). *J. Appl. Cryst.* **37**, 513–522.
Murshudov, G., Vagin, A. & Dodson, E. (1997). *Acta Cryst.* D**53**, 240–255.
Neutze, R., Wouts, R., der Spoel, D., Weckert, E. & Hadju, J. (2000). *Nature* (*London*), **406**, 752–757.

Ravelli, R. B. & McSweeney, S. M. (2000). *Structure*, **15**, 315–328.
Ravelli, R. B. G., Theveneau, P., McSweeney, S. & Caffrey, M. (2002). *J. Synchrotron Rad.* **9**, 355–360.
Sliz, P., Harrison, S. C. & Rosenbaum, G. (2003). *Structure*, **11**, 13–19.
Teng, T.-Y. & Moffat, K. (2000). *J. Synchrotron Rad.* **7**, 313–317.
Weik, M., Ravelli, R. B., Kryger, G., McSweeney, S., Raves, M. L., Harel, M., Gros, P., Silman, I., Kroon, J. & Sussman, J. L. (2000). *Proc. Natl Acad. Sci. USA*, **18**, 623–628.
Williams, P., Chaudhry, Y., Goodfellow, I. G., Billington, J., Powell, R., Spiller, O. B., Evans, D. J. & Lea, S. (2003). *J. Biol. Chem.* **278**, 10691–10696.